Strong first-order electroweak phase transition in the $U(1)_X$-extended MSSM

Shu-Min Zhao,[1,2,3,*] Jian-Fei Zhang,[1,2,3,†] Xi Wang,[1,2,3,‡] Xing-Xing Dong,[1,2,3,§] and Tai-Fu Feng[1,2,3,4,‖]

[1]*Department of Physics, Hebei University, Baoding 071002, China*
[2]*Key Laboratory of High-precision Computation and Application of Quantum Field Theory of Hebei Province, Baoding 071002, China*
[3]*Research Center for Computational Physics of Hebei Province, Baoding 071002, China*
[4]*Department of Physics, Chongqing University, Chongqing 401331, China*

(Received 25 October 2021; accepted 6 October 2023; published 30 October 2023)

In the $U(1)_X$ extension of the minimal supersymmetric standard model, there are three Higgs singlets and the corresponding trilinear terms in the Higgs effective potential. These new terms can allow a strongly first-order electroweak phase transition (EWPT) for a wide parameter space. We use codes CosmoTransitions to analyze the thermal evolution of the Higgs effective potential and calculate nucleation temperature. To find reasonable parameter spaces for strongly first-order EWPT, we randomly scan many parameters, which is numerically expensive. The diagrams are shown, that can lead to the 125 GeV Higgs mass and satisfy the first-order EWPT. This work benefits the phenomenology of $U(1)_X$ SSM and exploring new physics beyond the SM.

DOI: 10.1103/PhysRevD.108.075031

I. INTRODUCTION

Though the standard model (SM) has achieved great success for an excellent description of many experiment data in particle physics, it still fails to explain some puzzles: (1) It can not produce tiny mass to light neutrino [1]; (2) It can not provide a cold dark matter candidate; and (3) The observed baryon asymmetry of the Universe (BAU) is not explained in the SM [2]. On the supposition that the BAU is generated via the electroweak baryogenesis [3,4], the strong first-order electroweak phase transition (EWPT) is necessary to provide a nonequilibrium environment [5,6]. If the Higgs mass is less than 45 GeV, the strong EWPT can take place in the SM [5–7]. However, it conflicts with the present experiment data for the lightest CP-even Higgs mass $m_{h^0} = 125$ GeV. The SM CP-violation in the Cabibbo-Kobayashi-Maskawa matrix is so small that it is not able to generate a sufficient baryon asymmetry during the EWPT [2]. To solve this problem, the extension of SM with extra Higgs, heavy fermions, and supersymmetric extensions of SM are possible ways [7].

During the popular models of new physics, the minimal supersymmetric extension of the standard model (MSSM) [8] is a favorite one, which has been well-studied for many years. In the MSSM, there are additional sources of CP violation; the phases of μ and supersymmetric breaking parameters. To generate a strong first-order EWPT, the lightest stop-quark mass should be lighter than the top-quark mass $m_t \sim 173$ GeV, which is called the light stop scenario [9]. However, the current experimental constraint for the lightest stop-quark mass is $m_{\tilde{t}} > 1100$ GeV [10], so, this condition is ruled out by LHC constraints on stop masses.

With addition of the singlet S, the next-to-mimimal supersymmetric standard model (NMSSM) [11] has a trilinear term $\lambda A_\lambda S H_u H_d$ in the Higgs potential. In this condition, a strong enough first-order EWPT is allowed to occur [12]. In $U(1)$ gauge extensions of the MSSM [such as UMSSM and MSSM with $U(1)'$ symmetry], the EWPT is strongly first order for a wide parameter space [13]; the cost is introducing new extra singlet scalars, or adding new extra heavy singlet fermions.

Taking into account the shortcomings of the MSSM such as the μ problem and neutrino with zero mass, physicists extend the MSSM and obtain many new supersymmetric models, where the $U(1)$ extension is an interesting type [14]. There are some works of the strong first-order EWPT in the $U(1)$ extensions of the MSSM [15]. In this work, we add three Higgs singlets $\eta, \bar{\eta}, S$ and three generations of

*zhaosm@hbu.edu.cn
†zjf09@hbu.edu.cn
‡wangxi@stumail.hbu.edu.cn
§dxx_0304@163.com
‖fengtf@hbu.edu.cn

right-handed neutrinos to the $U(1)_X$ extension of the MSSM. This model is called as $U(1)_X$SSM with the local group $SU(3)_C \otimes SU(2)_L \otimes U(1)_Y \otimes U(1)_X$ [16,17]. The right-handed neutrinos and the added Higgs singlets produce several effects; light neutrinos obtain tiny masses through see-saw mechanism, right-handed neutrino possesses dark matter character, and scalar neutrino can be dark matter candidates. Comparing with the MSSM, the so called little hierarchy problem in $U(1)_X$SSM is relived because of the added superfields.

In the superpotential of $U(1)_X$SSM, there are two terms, $\mu\hat{H}_u\hat{H}_d$ and $\lambda_H\hat{S}\hat{H}_u\hat{H}_d$. Considering $\hat{S}$ with a nonzero vacuum expectation value (VEV) $(v_S/\sqrt{2})$, an effective $\mu_{\text{eff}} = \mu + \lambda_H v_S/\sqrt{2}$ is obtained, so it can relieve the μ problem. The $U(1)_X$SSM has three Higgs singlets and the corresponding trilinear terms. In the soft breaking terms, there are $B_S S^2$, $L_S S$, $\frac{T_\kappa}{3}S^3$, and $T_{\lambda_C} S\eta\bar{\eta}$, $\epsilon_{ij}T_{\lambda_H} S H_d^i H_u^j$, which appear in the Higgs effective potential. These new terms, especially the trilinear terms $(\frac{T_\kappa}{3}S^3, T_{\lambda_C}S\eta\bar{\eta}$, $\epsilon_{ij}T_{\lambda_H}SH_d^iH_u^j)$, can allow a strong first-order EWPT for a wide parameter space. We use codes CosmoTransitions [18] to analyze the thermal evolution of the effective potential and calculate the nucleation temperature. This model has more CP-violating sources than MSSM and can generate sufficient baryon asymmetry during EWPT.

At the critical temperature, the role of the global minimum of the potential passes from one local minimum to another, that is a necessary condition for a first-order phase transition. However, the critical temperature calculation does not account for the probability of the first-order phase transition actually taking place; via bubble nucleation, first-order phase transitions proceed. For the system transitioning from the false vacuum to the true vacuum, the probability is calculated through the bounce action [19]; the Euclidean space-time integral over the effective Lagrangian. The authors [20] find that analyzing only the vacuum structure via the critical temperatures can provide a misleading picture of the phase transition patterns, and of the parameter space so it is important to calculate the nucleation temperature to judge a successful strong first-order EWPT.

In Sec. II, we introduce the main content of $U(1)_X$SSM. The temperature corrections for the particle masses and the one loop effective potential at finite temperature are given out in Sec. III. We study the numerical results by codes CosmoTransitions and plot the figures in Sec. IV. The discussion and conclusion are shown in the last section.

II. THE $U(1)_X$SSM

Extending the local gauge group to $SU(3)_C \otimes SU(2)_L \otimes U(1)_Y \otimes U(1)_X$ and introducing three-generation right-handed neutrinos and three Higgs singlets to the MSSM, we obtain the $U(1)_X$ extension of MSSM, which is called as $U(1)_X$SSM. The right-handed neutrinos and Higgs singlets can solve the problem of light neutrino mass and mixing. The CP-even parts of the singlets $\eta, \bar{\eta}$, and S mix with the corresponding parts of H_u and H_d. Then the mass squared matrix of the neutral CP-even Higgs is extended to 5×5. The introduction of S can improve the lightest CP-even Higgs mass at tree level. One can find the particle contents in our previous work [16].

For $U(1)_X$SSM, the superpotential reads as

$$\begin{aligned} W = {} & l_W\hat{S} + \mu\hat{H}_u\hat{H}_d + M_S\hat{S}\,\hat{S} - Y_d\hat{d}\,\hat{q}\,\hat{H}_d - Y_e\hat{e}\,\hat{l}\,\hat{H}_d \\ & + \lambda_H\hat{S}\hat{H}_u\hat{H}_d + \lambda_C\hat{S}\,\hat{\eta}\,\hat{\bar{\eta}} + \frac{\kappa}{3}\hat{S}\,\hat{S}\,\hat{S} + Y_u\hat{u}\,\hat{q}\,\hat{H}_u \\ & + Y_X\hat{\nu}\,\hat{\bar{\eta}}\,\hat{\nu} + Y_\nu\hat{\nu}\,\hat{l}\,\hat{H}_u. \end{aligned} \tag{1}$$

The two Higgs doublets are same as those in MSSM,

$$\begin{aligned} & H_d = \begin{pmatrix} H_d^0 \\ H_d^- \end{pmatrix}, \qquad H_u = \begin{pmatrix} H_u^+ \\ H_u^0 \end{pmatrix}, \\ & H_d^0 = \frac{v_d + \phi_d^0 + iP_d^0}{\sqrt{2}}, \qquad H_u^0 = \frac{v_u + \phi_u^0 + iP_u^0}{\sqrt{2}}. \end{aligned} \tag{2}$$

$\tan\beta = v_u/v_d$ is defined by the VEVs of the Higgs superfields H_u and H_d.

The concrete forms of three Higgs singlets read as

$$\begin{aligned} & \eta = \frac{v_\eta + \phi_\eta^0 + iP_\eta^0}{\sqrt{2}}, \qquad \bar{\eta} = \frac{v_{\bar{\eta}} + \phi_{\bar{\eta}}^0 + iP_{\bar{\eta}}^0}{\sqrt{2}}, \\ & S = \frac{v_S + \phi_S^0 + iP_S^0}{\sqrt{2}}. \end{aligned} \tag{3}$$

v_η, $v_{\bar{\eta}}$, and v_S are the VEVs of the Higgs superfields η, $\bar{\eta}$, and S respectively. The β_η is defined as $\tan\beta_\eta = v_{\bar{\eta}}/v_\eta$.

The soft SUSY breaking terms of this model are shown as

$$\begin{aligned} \mathcal{L}_{\text{soft}} = {} & \mathcal{L}_{\text{soft}}^{\text{MSSM}} - B_S S^2 - L_S S - \frac{T_\kappa}{3}S^3 - T_{\lambda_C}S\eta\bar{\eta} \\ & + \epsilon_{ij}T_{\lambda_H}SH_d^iH_u^j - T_X^{IJ}\bar{\eta}\tilde{\nu}_R^{*I}\tilde{\nu}_R^{*J} + \epsilon_{ij}T_\nu^{IJ}H_u^i\tilde{\nu}_R^{I*}\tilde{l}_j^J \\ & - m_\eta^2|\eta|^2 - m_{\bar{\eta}}^2|\bar{\eta}|^2 - m_S^2S^2 - \left(m_{\tilde{\nu}_R}^2\right)^{IJ}\tilde{\nu}_R^{I*}\tilde{\nu}_R^J \\ & - \frac{1}{2}\left(M_S\lambda_{\tilde{X}}^2 + 2M_{BB'}\lambda_{\tilde{B}}\lambda_{\tilde{X}}\right) + \text{H.c.} \end{aligned} \tag{4}$$

We use $Y^{Y(X)}$ to denote the $U(1)_{Y(X)}$ charge, and the numbers of $Y^{Y(X)}$ for the superfields are given in our previous work [16]. We have proven that $U(1)_X$SSM is anomaly free. The gauge kinetic mixing is a new effect, which is produced by two Abelian groups $U(1)_Y$ and $U(1)_X$.

In the $U(1)_X$SSM, the covariant derivatives can be expressed as [21]

$$D_\mu = \partial_\mu - i\begin{pmatrix} Y^Y, & Y^X \end{pmatrix}\begin{pmatrix} g_Y, & g'_{YX} \\ g'_{XY}, & g'_X \end{pmatrix}\begin{pmatrix} A_\mu^{\prime Y} \\ A_\mu^{\prime X} \end{pmatrix}. \tag{5}$$

$A_\mu'^Y$ and $A_\mu'^X$ are the gauge fields of $U(1)_Y$ and $U(1)_X$. Because the two Abelian gauge groups are unbroken, we can rotate the gauge-coupling matrix with R [21] to make one nondiagonal element zero.

$$\begin{pmatrix} g_Y, & g'_{YX} \\ g'_{XY}, & g'_X \end{pmatrix} R^T = \begin{pmatrix} g_1, & g_{YX} \\ 0, & g_X \end{pmatrix}. \tag{6}$$

Three gauge bosons A_μ^X, A_μ^Y, and V_μ^3 mix together and produce a 3×3 mass squared matrix for neutral gauge bosons [22]. To diagonalize this matrix, two mixing angles θ_W and θ'_W are needed. $\sin^2\theta'_W$ is defined as [22]

$$\sin^2\theta'_W = \frac{1}{2} - \frac{\left((g_{YX}+g_X)^2 - g_1^2 - g_2^2\right)v^2 + 4g_X^2\xi^2}{2\sqrt{\left((g_{YX}+g_X)^2 + g_1^2 + g_2^2\right)^2 v^4 + 8g_X^2\left((g_{YX}+g_X)^2 - g_1^2 - g_2^2\right)v^2\xi^2 + 16g_X^4\xi^4}}. \tag{7}$$

The eigenvalues of the mass-squared matrix for neutral gauge bosons are deduced. One is zero mass corresponding to the photon. The other two values are for Z and Z'

$$\begin{aligned} m^2_{Z,Z'} = \frac{1}{8}\Big(& \left(g_1^2 + g_2^2 + (g_{YX}+g_X)^2\right)v^2 + 4g_X^2\xi^2 \\ & \mp \sqrt{\left(g_1^2 + g_2^2 + (g_{YX}+g_X)^2\right)^2 v^4 + 8\left((g_{YX}+g_X)^2 - g_1^2 - g_2^2\right)g_X^2 v^2\xi^2 + 16g_X^4\xi^4}\Big). \end{aligned} \tag{8}$$

Here, $v = \sqrt{v_u^2 + v_d^2}$ and $\xi = \sqrt{v_\eta^2 + v_{\bar\eta}^2}$.

At tree level, the Higgs potential is deduced [16]

$$\begin{aligned} V_0 = & \frac{1}{2}g_X(g_X+g_{YX})(|H_d^0|^2 - |H_u^0|^2)(|\eta|^2 - |\bar\eta|^2) + |\lambda_H|^2|H_u^0 H_d^0|^2 + m_s^2|S|^2 \\ & + \frac{1}{8}\left(g_1^2 + g_2^2 + (g_X+g_{YX})^2\right)(|H_d^0|^2 - |H_u^0|^2)^2 + \frac{1}{2}g_X^2(|\eta|^2 - |\bar\eta|^2)^2 + \lambda_C^2|\eta\bar\eta|^2 \\ & + (|\mu|^2 + |\lambda_H|^2|S|^2 + 2\mathrm{Re}[\mu^*\lambda_H S])(|H_d^0|^2 + |H_u^0|^2) + |\lambda_C|^2|S|^2(|\eta|^2 + |\bar\eta|^2) \\ & + 2\mathrm{Re}[l_W^*(2M_S S + \lambda_C\eta\bar\eta - \lambda_H H_u^0 H_d^0 + \kappa S^2)] + 4|M_S|^2|S|^2 + 2\mathrm{Re}[\lambda_C^*\kappa\eta^*\bar\eta^* S^2] \\ & + |\kappa|^2|S|^4 + 4\mathrm{Re}[M_S^* S^*(\lambda_C\eta\bar\eta - \lambda_H H_u^0 H_d^0 + \kappa S^2)] - 2\mathrm{Re}[\lambda_C^*\lambda_H\eta^*\bar\eta^* H_u^0 H_d^0] + |l_W|^2 \\ & - 2\mathrm{Re}[B_\mu H_d^0 H_u^0] + 2\mathrm{Re}[L_S S] + \frac{2}{3}\mathrm{Re}[T_k S^3] + 2\mathrm{Re}[T_{\lambda_C}\eta\bar\eta S] - 2\mathrm{Re}[T_{\lambda_H} H_d^0 H_u^0 S] \\ & - 2\mathrm{Re}[\lambda_H\kappa^* H_u^0 H_d^0 (S^2)^*] + m_\eta^2|\eta|^2 + m_{\bar\eta}^2|\bar\eta|^2 + m_{H_u^0}^2|H_u|^2 + m_{H_d}^2|H_d|^2 + 2\mathrm{Re}[B_S S^2]. \end{aligned} \tag{9}$$

The parameters $(\mu, \lambda_H, \lambda_C, l_W, M_S, B_\mu, L_S, T_\kappa, T_{\lambda_C}, T_{\lambda_H}, \kappa, B_S)$ in Eq. (9) are assumed to be real parameters to simplify the discussion. Through the formula

$$\left\langle \frac{\partial V_{\text{tree}}}{\partial H_u^0} \right\rangle = \left\langle \frac{\partial V_{\text{tree}}}{\partial H_d^0} \right\rangle = \left\langle \frac{\partial V_{\text{tree}}}{\partial \eta} \right\rangle = \left\langle \frac{\partial V_{\text{tree}}}{\partial \bar\eta} \right\rangle = \left\langle \frac{\partial V_{\text{tree}}}{\partial S} \right\rangle = 0, \tag{10}$$

one can obtain the following tadpole equations [16]

$$\begin{aligned} & \frac{v_d^2 - v_u^2}{8}\left(g_1^2 + g_2^2 + (g_X+g_{YX})^2\right) + \frac{g_X}{4}(g_X+g_{YX})(v_\eta^2 - v_{\bar\eta}^2) + \mu^2 + \frac{\lambda_H^2}{2}(v_u^2 + v_S^2) + m_{H_d}^2 \\ & + \sqrt{2}\mu\lambda_H v_S - \left[\lambda_H\left(\sqrt{2}M_S v_S + l_W + \frac{\lambda_C}{2}v_\eta v_{\bar\eta} + \frac{\kappa}{2}v_S^2\right) + B_\mu + \frac{T_{\lambda_H}}{\sqrt{2}}v_S\right]\tan\beta = 0, \end{aligned} \tag{11}$$

$$\frac{v_u^2-v_d^2}{8}\left(g_1^2+g_2^2+(g_X+g_{YX})^2\right)+\frac{g_X}{4}(g_X+g_{YX})(v_{\bar{\eta}}^2-v_\eta^2)+\mu^2+\frac{\lambda_H^2}{2}(v_S^2+v_d^2)+m_{H_u}^2$$
$$+\sqrt{2}\mu\lambda_H v_S-\left[\lambda_H\left(\sqrt{2}M_S v_S+l_W+\frac{\lambda_C}{2}v_\eta v_{\bar{\eta}}+\frac{\kappa}{2}v_S^2\right)+B_\mu+\frac{T_{\lambda_H}}{\sqrt{2}}v_S\right]\cot\beta=0, \tag{12}$$

$$\frac{g_X^2}{2}(v_\eta^2-v_{\bar{\eta}}^2)-\frac{g_X}{4}(g_X+g_{YX})(v_u^2-v_d^2)+\frac{\lambda_C^2}{2}(v_S^2+v_{\bar{\eta}}^2)+m_\eta^2+\left[\lambda_C\left(l_W+\sqrt{2}M_S v_S\right.\right.$$
$$\left.\left.-\frac{1}{2}\lambda_H v_u v_d+\frac{1}{2}\kappa v_S^2\right)+\frac{T_{\lambda_C}}{\sqrt{2}}v_S\right]\tan\beta_\eta=0, \tag{13}$$

$$\frac{1}{2}g_X^2(v_{\bar{\eta}}^2-v_\eta^2)+\frac{1}{4}g_X(g_X+g_{YX})(v_u^2-v_d^2)+\frac{1}{2}\lambda_C^2(v_S^2+v_\eta^2)+m_{\bar{\eta}}^2+\left[\lambda_C\left(l_W+\sqrt{2}M_S v_S\right.\right.$$
$$\left.\left.-\frac{1}{2}\lambda_H v_u v_d+\frac{1}{2}\kappa v_S^2\right)+\frac{T_{\lambda_C}}{\sqrt{2}}v_S\right]\cot\beta_\eta=0, \tag{14}$$

$$\frac{\lambda_H^2}{2}v^2+\frac{\lambda_C^2}{2}\xi^2+4M_S^2+\kappa(\kappa v_S^2+2l_W+3\sqrt{2}M_S v_S+\lambda_C v_\eta v_{\bar{\eta}}-\lambda_H v_u v_d)+\frac{T_k v_S}{\sqrt{2}}+2B_S$$
$$+m_S^2+\left[L_S+M_S(2l_W+\lambda_C v_\eta v_{\bar{\eta}}-\lambda_H v_u v_d)+\frac{\mu\lambda_H v^2+T_{\lambda_C}v_\eta v_{\bar{\eta}}-T_{\lambda_H}v_u v_d}{2}\right]\frac{\sqrt{2}}{v_S}=0. \tag{15}$$

III. THE ONE LOOP EFFECTIVE POTENTIAL AT FINITE TEMPERATURE

To simplify the discussion, we change the tree level potential V_0 in Eq. (9) to the form $V_0(h,y,z)$ with the relations

$$h^2=(\phi_d^0)^2+(\phi_u^0)^2,\qquad y^2=(\phi_\eta^0)^2+(\phi_{\bar{\eta}}^0)^2,$$
$$z^2=(\phi_S^0)^2,\qquad \frac{\phi_u^0}{\phi_d^0}=\tan\beta,\qquad \frac{\phi_{\bar{\eta}}^0}{\phi_\eta^0}=\tan\beta_\eta. \tag{16}$$

The one-loop effective potential at finite temperature [23] can be written in the following form [7]

$$V_{\rm eff}(h,y,z,T)=V_0(h,y,z)+V_1(h,y,z,0)+\Delta V_1(h,y,z,T)+\Delta V_{\rm daisy}(h,y,z,T). \tag{17}$$

Here, $V_0(h,y,z)$ is the tree-level potential. The one-loop zero-temperature correction is represented by $V_1(h,y,z,0)$ [24]. $\Delta V_1(h,y,z,T)$ represents the temperature-dependent one-loop correction [25], while $\Delta V_{\rm daisy}(h,y,z,T)$ denotes the multiloop daisy correction [26].

The concrete forms of $V_1(h,y,z,0)$, $\Delta V_1(h,y,z,T)$, and $\Delta V_{\rm daisy}(h,y,z,T)$ are shown explicitly

$$V_1(h,y,z,0)=\sum_i\frac{n_i}{64\pi^2}m_i^4(h,y,z)\times\left(\log\frac{m_i^2(h,y,z)}{Q^2}-C_i\right),$$
$$\Delta V_1(h,y,z,T)=\frac{T^4}{2\pi^2}\left\{\sum_i n_i J_i\left[\frac{m_i^2(h,y,z)}{T^2}\right]\right\},$$
$$\Delta V_{\rm daisy}(h,y,z,T)=-\frac{T}{12\pi}\sum_{i=\rm bosons}n_i\left[\mathcal{M}_i^3(h,y,z,T)-m_i^3(h,y,z)\right]. \tag{18}$$

In the zero-temperature correction, Q is the renormalization scale and assumed to be at TeV order. $m_i(h,y,z)$ denote field-dependent masses and n_i are the number of degrees of freedom. In Eq. (18), the particle masses m_i include fermions and bosons. The considered fermions are quarks $(t,\ b)$, lepton (τ), charginos, neutralinos, and neutrinos. While, the considered bosons are up-type squarks, down-type squarks, sleptons, CP-even sneutrinos, CP-odd sneutrinos, CP-even Higgs, CP-odd Higgs, Goldstones, vector bosons $(W^\pm,Z,Z')$. n_i are the degrees of freedom for the corresponding mass eigenstates. In $U(1)_X$SSM, the concrete values for n_i are the following: for quarks $n_i=-12$, for leptons and charginos $n_i=-4$, for neutralinos and neutrinos $n_i=-2$; for squarks $n_i=6$, for sleptons and charged Higgs (Goldstones) $n_i=2$, for Z and Z' bosons $n_i=3$, for W bosons $n_i=6$. for CP-odd, CP-even sneutrinos and the remaining Higgs scalars (Goldstones) $n_i=1$. The contents C_i depend on the regularization scheme. In the $\overline{\rm MS}$ scheme, they are assumed as $C_i=\frac{3}{2}$

for scalars and fermions and $C_i = \frac{5}{6}$ for gauge bosons. There is no evidence of the Goldstone catastrophe in the potential of this model. As discussed in Refs. [27–29], the IR divergences are spurious and can be tamed through resummation.

For bosons and fermions, the J_i functions in the one-loop effective potential at finite temperature have different forms [7,30]

$$J_B\left[m_B^2(h,y,z)/T^2\right] = \int_0^\infty dx x^2 \log\left\{1-\exp\left[-\sqrt{x^2+m_B^2(h,y,z)/T^2}\right]\right\},$$
$$J_F\left[m_F^2(h,y,z)/T^2\right] = \int_0^\infty dx x^2 \log\left\{1+\exp\left[-\sqrt{x^2+m_F^2(h,y,z)/T^2}\right]\right\}. \quad (19)$$

At high temperature and low temperature, the functions $J_B[m_B^2(h,y,z)/T^2]$ and $J_F[m_F^2(h,y,z)/T^2]$ can be expanded [5–7]. In the numerical calculation of Ref. [7], the authors give perfect approximations for the functions $J_B[m_B^2(h,y,z)/T^2]$ and $J_F[m_F^2(h,y,z)/T^2]$.

Adding temperature dependent self-energy contributions $\Pi(T)$ to $m_i^2(h,y,z)$, one can obtain the temperature dependent scalar mass squared $\mathcal{M}^2(h,y,z,T) = m^2(h,y,z) + \Pi(T)$ [31]. In this equation, $\Pi(T)$ is proportional to T^2. The longitudinal components of gauge bosons receive such contributions. The $\Pi(T)$ for particles in $U(1)_X$SSM are shown here. Following the method [7,31] for the temperature correction of particle mass, we deduce Eqs. (20)–(23) in our model:

(1) $\Pi(T)$ for scalar quarks,

$$\Pi_{\tilde{Q}_i}(T) = \left(\frac{2}{3}g_3^2+\frac{3}{8}g_2^2+\frac{1}{72}g_1^2+\frac{1}{4}(Y_{u_i}^2+Y_{d_i}^2)\right)T^2,$$
$$\Pi_{\tilde{u}_R^i}(T) = \left(\frac{2}{3}g_3^2+\frac{2}{9}g_1^2+\frac{1}{2}Y_{u_i}^2+\frac{1}{8}g_X^2\right)T^2,$$
$$\Pi_{\tilde{d}_R^i}(T) = \left(\frac{2}{3}g_3^2+\frac{1}{18}g_1^2+\frac{1}{2}Y_{d_i}^2+\frac{1}{8}g_X^2\right)T^2. \quad (20)$$

(2) $\Pi(T)$ for scalar charged leptons and scalar neutrinos,

$$\Pi_{\tilde{L}_i}(T) = \left(\frac{3}{8}g_2^2+\frac{1}{8}g_1^2+\frac{1}{4}Y_{e_i}^2\right)T^2, \qquad \Pi_{\tilde{e}_R^i}(T) = \left(\frac{1}{2}g_1^2+\frac{1}{2}Y_{e_i}^2+\frac{1}{8}g_X^2\right)T^2,$$
$$\Pi_{\tilde{\nu}_R^i}(T) = \left(\frac{1}{4}Y_X^2+\frac{1}{8}g_X^2\right)T^2. \quad (21)$$

(3) $\Pi(T)$ for Higgs doublets and singlets

$$\Pi_{H_d}(T) = \left(\frac{3}{8}g_2^2+\frac{1}{8}g_1^2+\frac{3}{4}Y_b^2+\frac{1}{8}g_X^2+\frac{1}{4}Y_{e_3}^2+\frac{1}{4}\lambda_H^2\right)T^2,$$
$$\Pi_{H_u}(T) = \left(\frac{3}{8}g_2^2+\frac{1}{8}g_1^2+\frac{3}{4}Y_t^2+\frac{1}{8}g_X^2+\frac{1}{4}\lambda_H^2\right)T^2, \qquad \Pi_\eta(T) = \left(\frac{1}{2}g_X^2+\frac{1}{4}\lambda_C^2\right)T^2,$$
$$\Pi_{\bar{\eta}}(T) = \left(\frac{1}{2}g_X^2+\frac{1}{4}\lambda_C^2+\frac{1}{4}\lambda_X^2\right)T^2, \qquad \Pi_S(T) = \left(\frac{1}{4}\kappa^2+\frac{1}{4}\lambda_C^2+\frac{1}{2}\lambda_H^2\right)T^2. \quad (22)$$

(4) $\Pi(T)$ for the longitudinal components of gauge bosons,

$$\Pi_{g_3}(T) = \frac{9}{2}g_3^2T^2, \qquad \Pi_{g_2}(T) = \frac{9}{2}g_2^2T^2,$$
$$\Pi_{g_1}(T) = \frac{11}{2}g_1^2T^2, \qquad \Pi_{g_X}(T) = \frac{9}{2}g_X^2T^2. \quad (23)$$

At finite temperature, the effective potential receives the thermal corrections. The tree-level cubic term and the loop corrections can produce interesting effects on the phase transition. To study the first-order EWPT better, we do not adopt the high-temperature approximation. Using the codes CosmoTransitions, we research the one-loop effective potential at finite temperature shown as Eq. (17). The codes CosmoTransitions can calculate the important parameters of phase transition, such as the critical temperature, the nucleation temperature, the step and type of phase transition, and the action, etc.

The phase transition can be a first-order EWPT, because there is a potential with barrier between the two minima. It is a tunneling process. Through nucleations of electroweak

bubbles which expand, collide, and coalesce, the transition proceeds and in the end the Universe turns into electroweak symmetry breaking phase. Through the first-order EWPT, baryon asymmetry can be generated from electroweak baryogenesis. The sphaleron process in the bubble should be sufficiently suppressed so as to preserve the generated baryon asymmetry after the EWPT. This requirement can be expressed as [7]

$$\frac{v(T_n)}{T_n} \gtrsim 1, \tag{24}$$

where T_n is the nucleation temperature. In the SM, $v(T)$ represents the VEV of the Higgs field H^0 at temperature T. In the MSSM, the condition is similar

$$v(T) = \sqrt{v_d^2(T) + v_u^2(T)}. \tag{25}$$

Here, $v_d(T)$ and $v_u(T)$ are the VEVs of the two neutral Higgs H_d^0 and H_u^0. The condition of $U(1)_X$SSM is more complex than that of MSSM, because three Higgs singlets are added.

Bubble nucleation is a random event. There is always a possibility of bubble nucleation. If the following condition is satisfied, there is one bubble generate in a Hubble volume, and the transition is able to complete,

$$S_E(T_n)/T_n \simeq 140, \tag{26}$$

where S_E represents the Euclidean bubble action.

IV. NUMERICAL RESULTS

Considering our previous works in the $U(1)_X$SSM [16], we study the numerical results in this section. The mass of the new neutral gauge boson is strict, and we take $M_{Z'} > 4.5$ TeV [16]. It is at 99% CL, that $\frac{M_{Z'}}{g_X} \geq 6$ TeV [32] for the ratio between $M_{Z'}$ and its gauge coupling. LHC experiment gives constraint for the new angle β_η as $\tan\beta_\eta < 1.5$ [33]. As a concrete example, we take the following parameters as

$$\begin{aligned}
&\tan\beta = 20, \quad Y_X = 1, \quad M_1 = 0.8\ \text{TeV}, \quad M_2 = 1.2\ \text{TeV}, \quad T_\kappa = 1.6\ \text{GeV},\\
&M_{BL} = T_{L_{ii}} = T_{\nu_{ii}} = T_X = T_{u_{ii}} = T_{d_{ii}} = 1\ \text{TeV}, \quad B_S = -1\ \text{TeV}^2,\\
&B_\mu = 1\ \text{TeV}^2, \quad M_{\tilde{Q}_{ii}}^2 = 3.5\ \text{TeV}^2, \quad M_{\tilde{U}_{ii}}^2 = 3\ \text{TeV}^2, \quad M_{\tilde{D}_{ii}}^2 = 4.5\ \text{TeV}^2,\\
&M_{\tilde{L}_{ii}}^2 = 0.5\ \text{TeV}^2, \quad M_{\tilde{E}_{ii}}^2 = 3\ \text{TeV}^2, \quad M_{\tilde{\nu}_{ii}}^2 = 0.2\ \text{TeV}^2, \quad l_W = 4\ \text{TeV}^2.
\end{aligned} \tag{27}$$

In order to find the parameter space satisfying the first-order EWPT, we use the following parameters as variables with their value ranges:

$$\begin{aligned}
&0.3 \leq g_X \leq 0.8, \quad 0.01 \leq g_{YX} \leq 0.5, \quad 0.1 \leq \kappa \leq 1.1, \quad -3\ \text{TeV} \leq T_{\lambda_C} \leq 3\ \text{TeV},\\
&-3\ \text{TeV} \leq T_{\lambda_H} \leq 3\ \text{TeV}, \quad 0.5\ \text{TeV} \leq M_S \leq 4\ \text{TeV}, \quad -1 \leq \lambda_H \leq 1, \quad -1 \leq \lambda_C \leq 1,\\
&0.6\ \text{TeV} \leq \mu \leq 1.5\ \text{TeV}, \quad -10\ \text{TeV}^3 \leq L_S \leq 10\ \text{TeV}^3, \quad 0.75 \leq \tan\beta_\eta \leq 0.99.
\end{aligned} \tag{28}$$

Some parameters such as $m_{H_u}^2$, $m_{H_d}^2$, m_η^2, $m_{\bar{\eta}}^2$ can be calculated from the tadpole equations [16] and the zero temperature correction. Using the codes CosmoTransitions, we study the phase transition in the $U(1)_X$SSM. We do not collect the results of the second phase transition, because they are not useful for the first-order EWPT and the numerical results are so computationally expensive. The showed plots are all suit for the first-order EWPT.

In Fig. 1 we show the plots calculated from the codes CosmoTransitions. The meanings of the red dot, the yellow dot, the green dot, and the blue dot are collected in the Table I. The points plotted by green dots and blue dots can lead to 125 GeV Higgs mass, where blue dots denote the parameters for strong first-order EWPT and green dots represent the condition of the weak first-order EWPT. For green dots and blue dots, the corresponding phase transitions are all 1 step in our obtained parameter space. Red dots and yellow dots represent the points for weak and strong first-order EWPT, respectively, without satisfying the constraint from the 125 GeV Higgs mass. The phase transitions denoted by red dots and yellow dots include 1-step, 2-step, and 3-step first-order EWPT [34], where 1-step first-order EWPTs are dominant. Because they do not satisfy the Higgs mass constraint, we do not further distinguish between them. The strongly first-order EWPT is of interest, and the nucleation temperature is obtained from the codes CosmoTransitions.

Figure 1(a) shows the plots in the plane of g_X and λ_H. g_X is the $U(1)_X$ gauge coupling constant. λ_H is the constant for the term $\lambda_H \hat{S}\hat{H}_u\hat{H}_d$ in the super potential. g_X and λ_H both appear in the mass squared matrix of CP-even Higgs at tree level. Therefore, they are both important parameters.

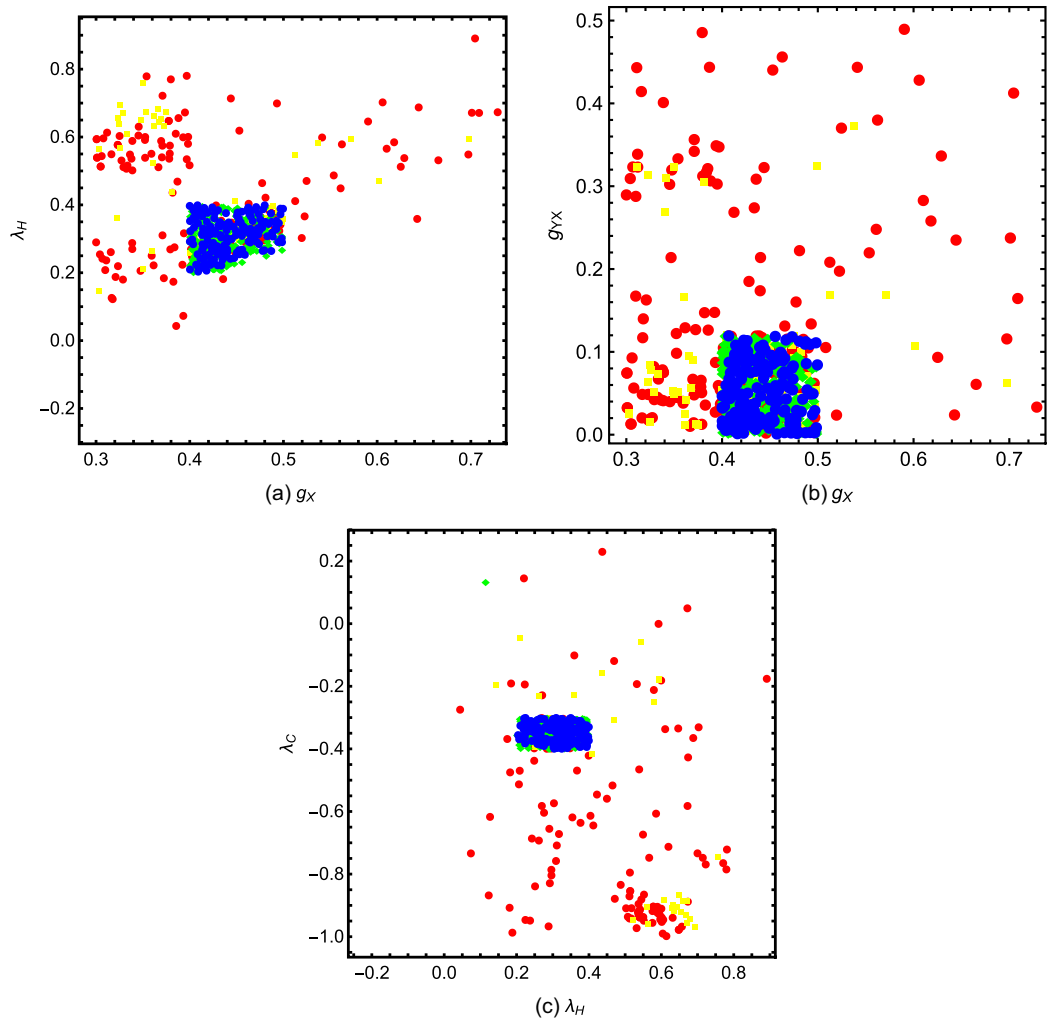

FIG. 1. The diagram (a) shows the points in the plane of g_X versus λ_H. The diagram (b) shows the points in the plane of g_X versus g_{YX}. The diagram (c) shows the points in the plane of λ_H versus λ_C.

The four type points are in the region $\lambda_H > 0$. During the g_X range $0.3 \leq g_X \leq 0.5$, there are more points. Green dots and blue dots are concentrated in a small area with $0.4 \leq g_X \leq 0.5$ and $0.2 \leq \lambda_H \leq 0.4$, because these results are constrained by the 125 GeV Higgs mass. The blue area looks like a trapezium, which is better than the other area.

Figure 1(b) is shown in the plane of g_X and g_{YX}. g_{YX} is the coupling constant for gauge mixing of $U(1)_Y$ and $U(1)_X$, which is a new parameter beyond MSSM and can bring new effects. Though the points appear in almost the whole region of the plane, they concentrate in the bottom left corner with $0.3 \leq g_X \leq 0.5$ and $0 \leq g_{YX} \leq 0.18$. In the square area $0.4 \leq g_X \leq 0.5$ and $0 \leq g_{YX} \leq 0.1$, there are a lot of blue dots.

In Fig. 1(c), the four types plots are shown in the plane of λ_H and λ_C. λ_C emerges in the term $\lambda_C \hat{S}\hat{\eta}\hat{\bar{\eta}}$ of the superpotential. Because η and $\bar{\eta}$ are Higgs singlets, the term including λ_C give contributions to the CP-even Higgs mass squared matrix. Then λ_C should influence Higgs mass to some extent. All the points of the numerical results are

TABLE I. The markers in numerical results.

Shape style	Weak first-order EWPT	Strong first-order EWPT	125 GeV Higgs mass
Red dot	✓	✗	✗
Yellow dot	✗	✓	✗
Green dot	✓	✗	✓
Blue dot	✗	✓	✓

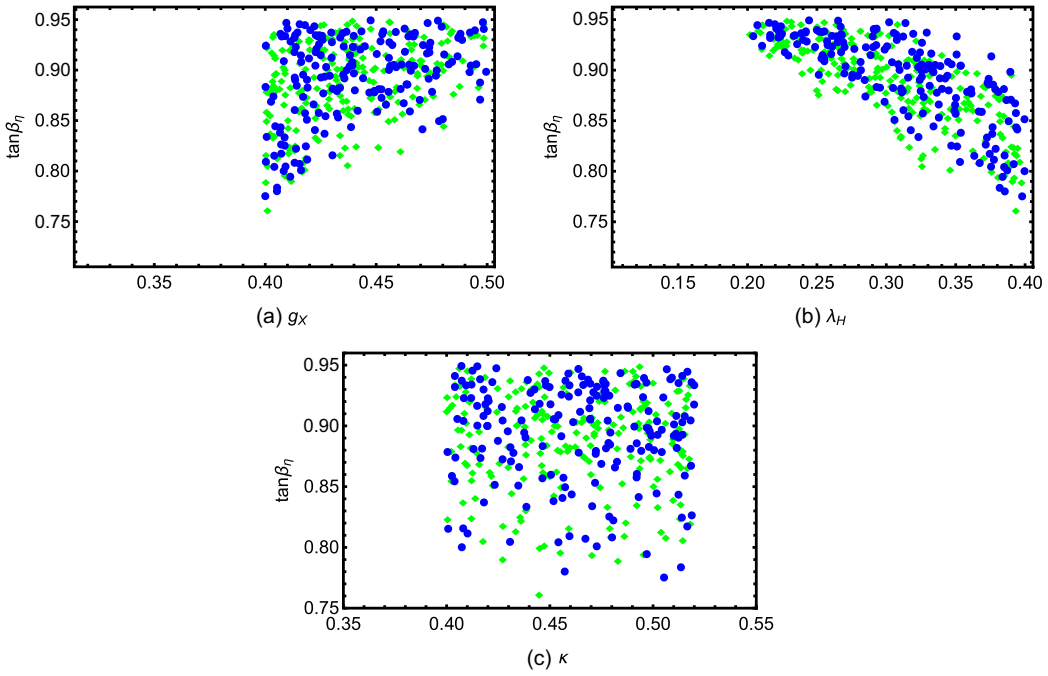

FIG. 2. Diagram (a) shows the points in the plane of g_X versus $\tan\beta_\eta$. Diagram (b) shows the points in the plane of λ_H versus $\tan\beta_\eta$. Diagram (c) shows the points in the plane of κ versus $\tan\beta_\eta$.

scattered in most areas. Most red dots appear in the area $0.1 \leq \lambda_H \leq 0.8$ and $-1.0 \leq \lambda_C \leq -0.3$. Obviously, blue dots are concentrated in much a smaller region, $0.2 \leq \lambda_H \leq 0.4$ and $-0.3 \leq \lambda_C \leq -0.4$, because blue dots obey the constraint from the 125 GeV Higgs mass, and it is reasonable.

Since the results represented by red dots and yellow dots do not lead to 125 GeV Higgs mass, we do not show them in the following figure. Then, only blue dots and green dots are plotted in latter analysis. The parameter $\tan\beta_\eta$ affects the masses of many particles including Higgs, and appears in the Higgs potential at tree level. Therefore, it should bring obvious effect on the phase transition. Figure 2(a) embodies blue dots and green dots in the plane of g_X versus $\tan\beta_\eta$. The points look like a right trapezoid in the whole. Most blue dots concentrate in the area $0.4 \leq g_X \leq 0.5$ and $0.85 \leq \tan\beta_\eta \leq 0.95$. When $\tan\beta_\eta < 0.85$, the both type points decrease quickly.

To see the effects of λ_H and $\tan\beta_\eta$, blue dots and green dots are shown in Fig. 2(b). All the points appear at the top-right corner of this diagram, and most of the space is blank, especially the bottom-left corner. It implies that the constraints from both 125 GeV Higgs and first-order EWPT are strict.

Figure 2(c) is shown in the plane of κ versus $\tan\beta_\eta$. κ is the parameter in the term $\frac{1}{3}\kappa\hat{S}\,\hat{S}\,\hat{S}$ of the superpotential. κ has relation with the Higgs tree-level potential and Higgs mass matrix through the mixing with Higgs singlet $\hat{S}$. From analytical analysis, κ should affect the Higgs and phase transition to some extent but not strong. This diagram is exactly what is reflected. The dots become fewer and fewer from top to bottom. It implies that the effect of $\tan\beta_\eta$ is stronger than that of κ obviously.

Blue dots and green dots represent the first-order EWPT that can take place. For these points, the nucleation temperature T_n and the Euclidean bubble action $S_E(T_n)$ are calculated through the codes CosmoTransitions. For the weak first-order EWPT points (green dots), the nucleation temperature T_n is relatively high and in the region from 650 to 1000 GeV. On the other hand, the nucleation temperature T_n of the strong first-order EWPT points (blue dots) is more reasonable. Most blue dots are located in the region $100\ \text{GeV} \leq T_n \leq 600\ \text{GeV}$, which implies strong first-order EWPT can, in fact, be realized. As T_n is defined as $S_E(T_n)/T_n = 140$, the numerical results for the ratios $S_E(T_n)/T_n$ of all the points (blue dots and green dots) are very close to 140. The distribution discrepancy is due to numerical errors.

V. DISCUSSION AND CONCLUSION

In the $U(1)_X$ extension of MSSM, we study the strong first-order EWPT. The Higgs singlets $\hat{\eta}, \hat{\bar{\eta}}$ and $\hat{S}$ are beyond MSSM, and they bring new terms to the Higgs potential. The one-loop effective potential at finite temperature is composed of four parts; the tree-level potential $V_0(h, y, z)$, the one-loop zero-temperature correction $V_1(h, y, z, 0)$, the temperature-dependent one-loop correction $\Delta V_1(h, y, z, T)$, and the multiloop daisy correction $\Delta V_{\text{daisy}}(h, y, z, T)$. The tree-level potential has $T_{\lambda_C} S\eta\bar{\eta}$, $\epsilon_{ij} T_{\lambda_H} S H_d^i H_u^j$ etc., coming from the soft breaking terms.

These terms go beyond the MSSM and allow the strong first-order EWPT to take place.

In the numerical calculation, we take the parameters considering the experiment constraints especially from the 125 GeV Higgs mass. At very high temperature, the global minimum is at the origin. As the temperature drops down, the phase transition takes place. Taking several parameters as variable, we scan the parameter space that can lead to 125 GeV Higgs mass and strong first-order EWPT. 1-step phase transitions are dominant, and the nucleation temperature T_n is reasonable for the strong first-order EWPT. The effects of added Higgs singlets for phase transition need more work, and we shall study them in the future.

ACKNOWLEDGMENTS

This work is supported by National Natural Science Foundation of China (NNSFC) (Grant No. 12075074), Natural Science Foundation of Hebei Province (Grants No. A202201022 and No. A2022201017), and the Natural Science Foundation of Hebei Education Department (Grant No. QN2022173).

[1] T2K Collaboration, Phys. Rev. Lett. **107**, 041801 (2011); MINOS Collaboration, Phys. Rev. Lett. **107**, 181802 (2011); DAYA-BAY Collaboration, Phys. Rev. Lett. **108**, 171803 (2012).
[2] A. I. Bochkarev and M. E. Shaposhnikov, Mod. Phys. Lett. A **02**, 417 (1987); K. Kajantie, M. Laine, and K. Rummukainen *et al.*, Nucl. Phys. **B466**, 189 (1996).
[3] V. A. Kuzmin, V. A. Rubakov, and M. E. Shaposhnikov, Phys. Lett. **155B**, 36 (1985); D. E. Morrissey and M. J. R. Musolf, New J. Phys. **14**, 125003 (2012).
[4] M. E. Shaposhnikov, Pis'ma Zh. Eksp. Teor. Fiz. **44**, 364 (1986) [JETP Lett. **44**, 465 (1986)].
[5] W. Chao, H. K. Guo, and J. Shu, J. Cosmol. Astropart. Phys. 09 (2017) 009.
[6] L. G. Bian, Y. C. Wu, and K. P. Xie, J. High Energy Phys. 12 (2019) 028.
[7] J. H. Kang, P. Langacker, and T. J. Li, and T. Liu, J. High Energy Phys. 04 (2011) 097.
[8] J. Rosiek, Phys. Rev. D **41**, 3464 (1990); H. P. Nilles, Phys. Rep. **110**, 1 (1984); H. E. Haber and G. L. Kane, Phys. Rep. **117**, 75 (1985).
[9] K. Funakubo and E. Senaha, Phys. Rev. D **79**, 115024 (2009); S. W. Ham, S. K. OH, and D. Son, Phys. Rev. D **71**, 015001 (2005).
[10] Particle Data Group, Prog. Theor. Exp. Phys. **2020**, 083C01 (2020).
[11] U. Ellwanger, C. Hugonie, and A. M. Teixeira, Phys. Rep. **496**, 1 (2010); J. Ellis, J. F. Gunion, H. E. Haber, L. Roszkowski, and F. Zwirner, Phys. Rev. D **39**, 844 (1989); J. J. Cao, J. Li, Y. S. Pan, L. Shang, Y. Yue, and D. Zhang, Phys. Rev. D **99**, 115033 (2019).
[12] S. J. Huber, T. Konstandin, T. Prokopec *et al.*, Nucl. Phys. **B757**, 172 (2006).
[13] D. Land and E. Carlson, Phys. Lett. B **292**, 107 (1992); S. Profumo, M. J. R. Musolf, and G. Shaughnessy, J. High Energy Phys. 08 (2007) 010.
[14] P. Bandyopadhyay, E. J. Chun, and J. C. Park, J. High Energy Phys. 06 (2011) 129; G. Belanger, J. D. Silva, and A. Pukhov, J. Cosmol. Astropart. Phys. 12 (2011) 014.
[15] A. Ahriche and S. Nasri, Phys. Rev. D **83**, 045032 (2011); S. W. Ham and S. K. OH, Phys. Rev. D **76**, 095018 (2007).
[16] S.-M. Zhao, T.-F. Feng, M.-J. Zhang, J.-L. Yang, H.-B. Zhang, and G.-Z. Ning, J. High Energy Phys. 02 (2020) 130; S. M. Zhao, G. Z. Ning, J. J. Feng *et al.*, Nucl. Phys. **B969**, 115469 (2021).
[17] F. Staub, Comput. Phys. Commun. **185**, 1773 (2014); Adv. High Energy Phys. **2015**, 840780 (2015).
[18] C. L. Wainwright, Comput. Phys. Commun. **183**, 2006 (2012).
[19] P. Athron, C. Balazs, A. Fowlie, G. Pozzo, G. White, and Y. Zhang, J. High Energy Phys. 11 (2019) 151.
[20] S. Baum, M. Carena, N. R. Shah, C. E. M. Wagner, and Y. Wang, J. High Energy Phys. 03 (2021) 055.
[21] V. Barger, P. F. Perez, and S. Spinner, Phys. Rev. Lett. **102**, 181802 (2009); G. Belanger, J. D. Silva, and H. M. Tran, Phys. Rev. D **95**, 115017 (2017).
[22] S. M. Zhao, L. H. Su, X. X. Dong, T.-T. Wang, and T.-F. Feng, J. High Energy Phys. 03 (2022) 101.
[23] M. E. Carrington, Phys. Rev. D **45**, 2933 (1992).
[24] S. R. Coleman, Phys. Rev. D **7**, 1888 (1973).
[25] M. Quiros, arXiv:hep-ph/9901312.
[26] R. R. Parwani, Phys. Rev. D **45**, 4695 (1992); **48**, 5965(E) (1993); D. J. Gross, R. D. Pisarski, and L. G. Yaffe, Rev. Mod. Phys. **53**, 43 (1981).
[27] J. E. Miro, J. R. Espinosa, and T. Konstandin, J. High Energy Phys. 08 (2014) 034.
[28] S. P. Martin, Phys. Rev. D **90**, 016013 (2014).
[29] P. Athron, C. Balazs, A. Fowlie, L. Morris, G. White, and Y. Zhang, J. High Energy Phys. 01 (2023) 050.
[30] D. Curtin, P. Meade, and H. Ramani, Eur. Phys. J. C **78**, 787 (2018).
[31] D. Comelli and J. R. Espinosa, Phys. Rev. D **55**, 6253 (1997); N. Haba and T. Yamada, Phys. Rev. D **101**, 075027 (2020).
[32] G. Cacciapaglia, C. Csaki, G. Marandella, and A. Strumia, Phys. Rev. D **74**, 033011 (2006); M. Carena, A. Daleo, and B. A. Dobrescu, and T. M. P. Tait, Phys. Rev. D **70**, 093009 (2004).
[33] L. Basso, Adv. High Energy Phys. **2015**, 980687 (2015).
[34] S. Inoue, G. Ovanesyan, and M. J. R. Musolf, Phys. Rev. D **93**, 015013 (2016); V. Vaskonen, Phys. Rev. D **95**, 123515 (2017).